High-Powered Operation of a Magnetically Expanding Plasma Using Permanent Magnets

Kaoru OGUNI, Kazunori TAKAHASHI, Yutaka SHIDA, and Tamiya FUJIWARA

Department of Electrical and Electronic Engineering, Iwate University, Morioka, Iwate 020-8551, Japan

(Received: 26 October 2009 / Accepted: 1 February 2010)

A solenoid-free, magnetically expanding plasma source using permanent magnets are operated for high radiofrequency-power of 13.56 MHz, where expanding magnetic fields of about one hundred gauss in the source tube and of a few gauss in the diffusion chamber are provided by double concentric arrays of the permanent magnets. The operating argon gas pressure is maintained at 1 mTorr in the present experiments. Under the present conditions, an electric double layer (DL) is spontaneously formed near the source exit and ions in the source tube are supersonically accelerated to the energy corresponding to the potential drop of the DL. The plasma density in the source tube can be increased up to 10^{12} cm^{-3} in the source tube for rf power of 1 kW, whereas the supersonic ion beam is hardly detected in the diffusion chamber for high-powered plasma above 600 W. For high-powered case, the magnetic fluctuation propagating in the diffusion chamber is found to create the bulk ions through the process of the ionization.

Keywords: radiofrequency plasma, helicon wave, double layer, ion acceleration, magnetically expanding plasma

1. Introduction

Inhomogeneously magnetized plasmas under divergent magnetic-field configurations, i.e., magnetic nozzle, have been investigated for a long time because the charged particles in the plasmas can be accelerated magnetohydrodynamically or electrostatically. The process of the magnetohydrodynamic plasma acceleration has been suggested to be utilized for development of high-power electric propulsion devices such as Variable Specific Impulse Magnetoplasma Rocket (VASIMR) [1], recent investigation on a Lissajous plasma acceleration proposed by Toki *et al.* [2], and so on. On the other hand, the electrostatic ion accelerations have recently been observed simultaneously with spontaneous formation of electric double layers (DLs) in the magnetically expanding radiofrequency (rf) plasmas, where the rapid potential drop is created near the exit of the plasma sources [3]. In the magnetically expanding plasmas containing the DLs, it has been reported that the energetic "free" electrons in the plasma source can overcome the potential drop of the DL and neutralize the supersonic ion beam accelerated by the DL in particle-in-cell simulation [4] and in experiments [5–7]. Since the particle behaviors in the DL plasmas are very similar to that in the ion engine used in MUSES-C mission [8] where the ions are accelerated by the grid electrode, the DL acceleration is also suggested to be useful for the long-lifetime propulsion devices [9].

The rf plasma sources under the steady-state magnetic fields have a potential application because of the achievement of highly dense plasma through the process of the helicon wave propagation and absorption [10–12]. In the conventional helicon sources, the electromagnets are used for generation of the steady-state magnetic fields as well as the magnetically expanding plasmas. For the purpose of the reduction of the consumed electric power, weight of the source, and the cost, permanent magnets (PMs) are introduced in the development of the helicon source [13–17]. One of the experiments using the PMs demonstrate that the DL is formed near the source exit and the ions are accelerated through the DL when the divergent magnetic fields are provided by the combination of the PMs and the electromagnets [15]. More recently, the DL-induced ion beam has been detected in the magnetically expanding plasma using only the PMs [18], where double concentric arrays of the PMs are employed to generate the constant magnetic fields in the source tube and divergent magnetic fields near the source exit. The expanding plasma source using only the PMs is considered to be useful for development of an efficient and long-lived propulsion devices.

In the previous works on the PMs-expanded plasma [18, 19], the rf power for plasma productions in argon is maintained at a few hundreds watt. In order to increase thrust obtained by this type of the propulsion device, the plasma density in the source and the ion beam energy corresponding to the potential drop of the DL are required to be increased. In the present paper, we report the high-powered operation of the PMs-expanded plasma source, where the rf

author's e-mail: kazunori@iwate-u.ac.jp

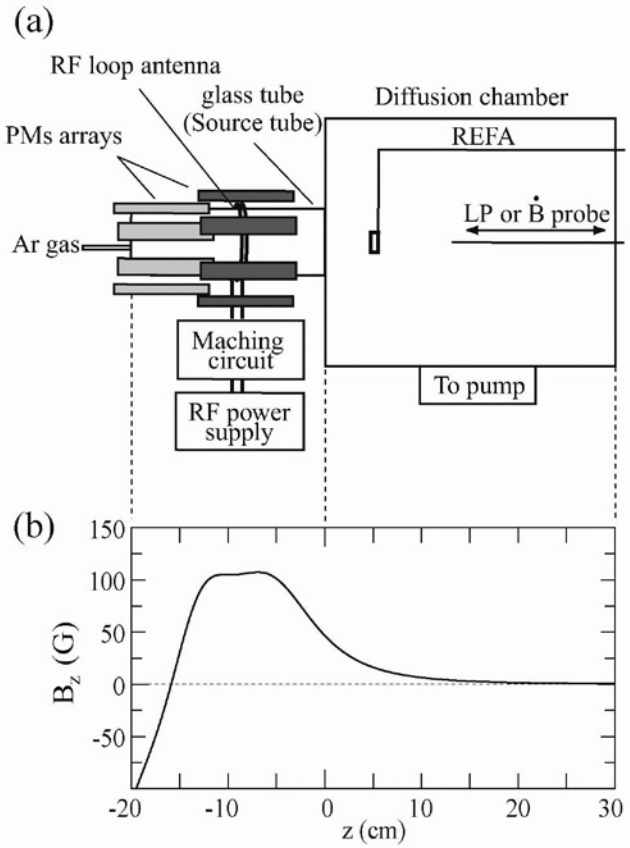

Fig. 1 (a) Schematic diagram of the experimental setup. (b) Calculated axial profile of the magnetic fields B_z provided by the double concentric arrays of the PMs, where the positive and negative signs of B_z show the magnetic-field lines facing the right and facing left in Fig. 1(a), respectively.

power is increased up to 1 kW under the condition of the maintained argon gas pressure of 1 mTorr. In the experiments, the plasma density in the source tube and ion energy distribution functions (IEDFs) downstream of the source exit are measured by a Langmuir probe (LP) and an retarding field energy analyzer (RFEA) [20]. Section 2 describes the experimental setup, and the experimental results are presented in Sec. 3. In Sec. 3, the supersonic ion beam is detected for low-powered operation of the source below 600 W. The results on the high-powered operation of the source show the increase in the plasma density up to 10^{12} cm^{-3} for 1 kW power, while the IEDFs for rf power higher than about 600 W barely show the accelerated group of ions. This phenomenon is discussed in Sec. 4 and conclusions are given in Sec. 5.

2. Experimental setup

Figure 1(a) shows the schematic diagram of the experimental setup of the PMs-expanded plasma machine, which has previously been described in Ref. [18]. Briefly, a cylindrical pyrex glass tube (source tube) 20 cm in length and 6.5 cm in inner diameter is contiguously connected to a 30-cm-long and 26-cm-diameter stainless steel vacuum chamber (diffusion chamber), which are evacuated to a base pressure of 10^{-6} Torr by a rotary/diffusion pumping system. Here, z is the axial position and $z = 0$ is defined as the interface between the source tube and the diffusion chamber, i.e., the source exit. The argon gas is introduced from the upstream flange of the source side through a mass flow controller and the gas pressure in the chamber is maintained at 1 mTorr in the present experiments. An argon plasma is excited by a 7-cm-diameter double-turn loop antenna located at $z = -9$ cm and powered from an rf generator of frequency 13.56 MHz through an impedance matching circuit. The forwarded and reflected rf power are monitored by the SWR (standing wave ratio) meter, which are inserted between the rf generator and the matching circuit in series, and the capacitors in the matching circuit are tuned to reduce the reflected power. In the present experiments, the SWR are confirmed to be equal to one for all conditions, which means that there is no rf-power reflected to the rf generator. The plasma inside the source tube is terminated by an insulator plate located in front of the upstream flange at $z = -20$ cm, which ensure the current-free mode operation of the source.

Surrounding the source tube, the double concentric arrays of Neodymium Iron Boron (NdFeB) permanent magnets (10 cm in length, 1.5 cm in width, and 0.5 cm in thickness) are set in order to generate the steady-state divergent magnetic fields for the formation of the DL. The detailed configuration of the PMs has previously been described in Ref. [18]; the configuration can produce the constant field area inside the source tube and the divergent magnetic fields near the source exit. The axial profile of the calculated axial component of the magnetic-field strength B_z are plotted in Fig. 1(b). According to Ref. [15], the cusp fields created by the PMs prevent the plasma diffusion, the formation of the DL, and the generation of the ion beam. As seen in Fig. 1(b), there is no cusp between the constant field area ($z = -13$ - -6 cm) and the diffusion chamber ($z > 0$ cm). Under the above-mentioned conditions, the rapid potential drop with thickness of a few centimeter and a few tens volts, i.e., the DL, and the subsequent ion beam have been observed for rf power $P_{RF} = 250$ W in the previous studies.

An axially movable LP with a planar tip and the RFEA are inserted from the downstream port of the diffusion chamber. The plasma density n_p can be estimated from the ion saturation current of the LP, which are derived as [21]

$$I_{is} = 0.61 S n_p e u_B, \tag{1}$$

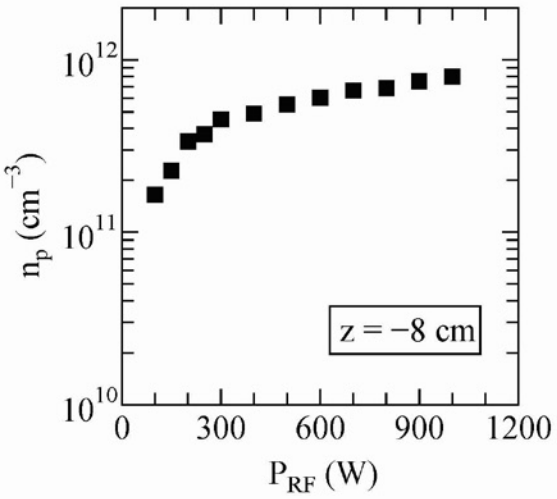

Fig. 2 The plasma density n_p as a function of the rf power P_{RF}, measured at $z = -8$ cm inside the source tube.

where S, e, and u_B are the collecting area of the LP, the elementary charge, and the Bohm velocity. The electron temperature measured in the diffusion chamber ($T_e \simeq 5$ eV) under the assumption that the electron energy distribution functions are Maxwellian [5], is used for the calculation of the Bohm velocity. The IEDFs are well know to be proportional to the first derivative of the I_c-V_c characteristic, i.e., dI_c/dV_c, which are measured using an active analog differentiator [22]. Outside the vacuum chamber, the collector electrode is electrically connected to 10 kΩ resistor and bipolar voltage supply in series, where the collector voltage V_c is linearly swept from −20 V to 120 V for about 25 msec. The current signal I_c converted into the voltage signal through the resister is fed through an isolation amplifier to the active analog circuit. The active analog circuit acts as a differentiator for the current signal during the slowly-swept voltage and as a filter for the plasma instabilities and the electric noise above about a few kHz. The signals are monitored and digitized by a digital storage oscilloscope (Tektronix TDS 2024B) with 1 MΩ input impedance, and passed into the Data Acquisition (DAQ) system. A magnetic probe ($\dot{B}$ probe) is also inserted from the downstream side for the measurement of magnetic fluctuation of 13.56 MHz, which are connected to the digital oscilloscope through 50 Ω terminator. The amplitude of the fluctuation can be obtained through Fourier analysis.

3. Experimental results

Figure 2 shows the plasma density n_p measured at $z = -8$ cm inside the source tube, as a function of the rf power P_{RF}, where the change of the electron temperature has not been observed from the current-voltage characteristics of the classical LP. Strictly speaking, the electron energy distribution or probability functions are required to be measured using the rf compensated probe as previously reported by Takahashi *et al.* [5], which is the next step of our studies. The plasma density is found to increase with an increase in the rf power P_{RF}, although the discontinuous jump of the plasma density [23, 24], i.e., the specific feature of the transition from the inductively coupled mode to the helicon wave mode discharges, has not been observed here. Apart from the matter on the discharge mode, the plasma density in the source tube is achieved to be increased up to 10^{12} cm^{-3} for $P_{RF} = 1$ kW.

For low-powered operation of the source, the previous experiments demonstrate the formation of the rapid potential drop like the DL structure at $z = -3$ - 1 cm and the subsequent generation of the ion beam. Figure 3 shows the IEDF parallel to the machine axis for $P_{RF} = 200$ W, measured at $z = 3$ cm downstream of the DL, which clearly shows the accelerated group of ions in addition to the thermal bulk ions. It is reported that the accelerated ions decay exponentially to the z axis with a decay constant close to the ion-neutral mean free path for charge exchange [19] ; this process yield the existence of the bulk ions in the side downstream of the DL. In the RFEA measurement, the low- and high-energy peaks indicate the existence of both the thermal and electrostatically accelerated ions. The collector voltages V_c yielding the low- and high-energy peaks give us the local plasma potential ϕ_p ($\sim$ 18 V) and the beam potential ϕ_{beam} ($\simeq$ 35 V) as indicated by arrows in Fig. 3, where note that the beam "potential" is different from the beam "en-

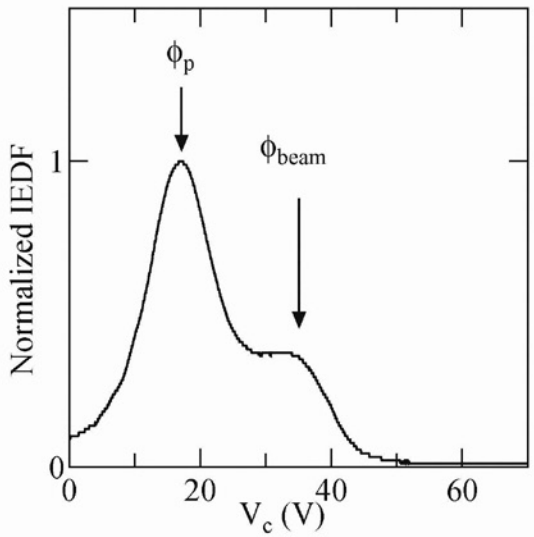

Fig. 3 The IEDF parallel to the machine axis for $P_{RF} =$ 200 W, measured at $z = 3$ cm downstream of the DL.

ergy" because the zero energy corresponds to the local plasma potential. According to the principle of the RFEA measurements, the energy ε_{beam} of the ion beam can be derived as

$$\varepsilon_{beam} = \phi_{beam} - \phi_p. \quad (2)$$

Hence, the energy of the ion beam can be identified as $\varepsilon_{beam} \sim 17$ eV, which agrees with the potential drop ϕ_{DL} of the DL [19]. The strength of the DL in the present experiments is found to be about three times of the electron temperature (~ 5 eV). The calculated ion sound speed for $T_e = 5$ eV is about 3.5 km/s. The velocity v_{beam} of the ion beam can be expressed as

$$v_{beam} = \sqrt{\frac{2e\varepsilon_{beam}}{M_i}}, \quad (3)$$

where M_i is the mass of the argon ion. The velocity of the ions with energy of 17 eV is $v_{beam} \sim 9.2$ km/s. Therefore, the observed ion beam is supersonic with the Mach number of about 2.6. These results are very close to the previously observed ion acceleration in the magnetically expanding plasma using the solenoid coils [25].

The IEDFs downstream of the source exit are measured for various rf power in the range of P_{RF} = 100 - 1000 W. Figure 4 shows the normalized IEDF parallel to the machine axis measured at $z = 3$ cm by the RFEA facing the source tube, as a function of the rf power P_{RF}, where the data for $P_{RF} = 100$ W, 500 W, and 1 kW are plotted as bold lines for clarity. For all the rf power in the range of 100 - 1000 W, the low-energy peak of the IEDF, indicating the local plasma potential, are observed at $V_c \sim 18$ V. The high-energy peak indicating the accelerated group of ions is clearly detected for comparatively low rf power below 500 W at $V_c \sim 35$ V, while it is found that the accelerated ions can barely be observed above 600 W.

The ion beam energies ε_{beam}, i.e., the difference between the local plasma potential and the beam potential, is estimated for each rf power as plotted in

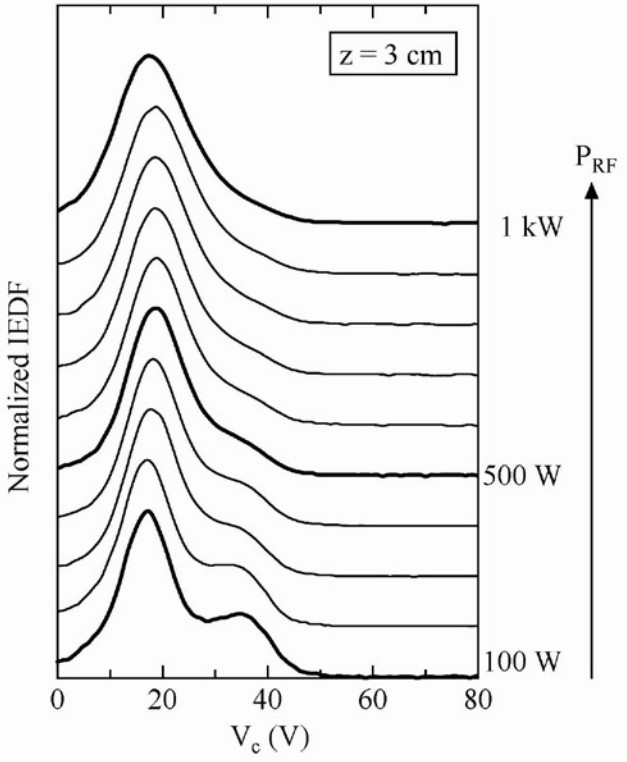

Fig. 4 The IEDF parallel to the machine axis, measured at $z = 3$ cm, as a function of the rf power P_{RF}. The bold lines in Fig. 4 corresponds to the data for $P_{RF} = 100$ W, 500 W, and 1 kW, respectively.

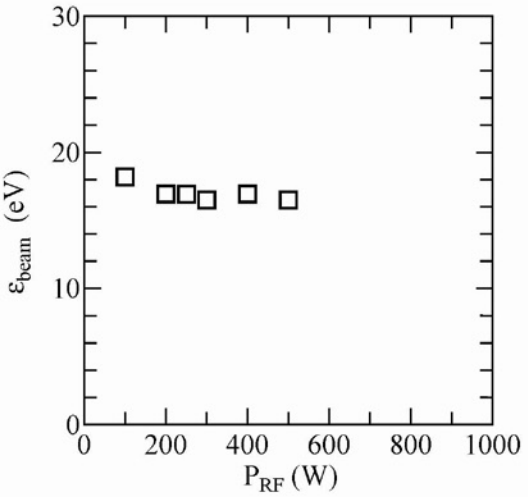

Fig. 5 The ion beam energy ε_{beam} identified from the experimental data shown in Fig. 4, as a function of the rf power P_{RF}, where the accelerated group of ions are hardly detected for the rf power above 500 W.

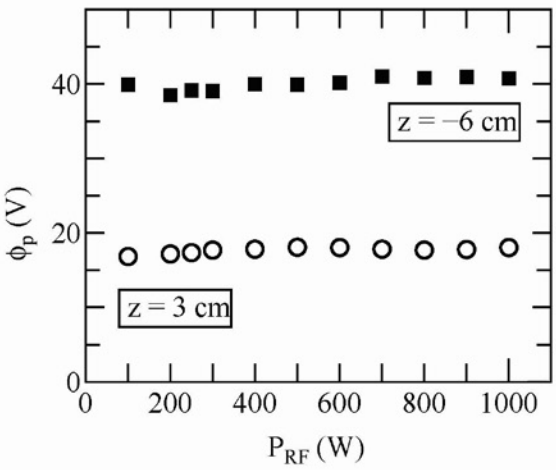

Fig. 6 The measured local plasma potentials ϕ_p inside the source tube ($z = -6$ cm: closed squares) and in the diffusion chamber ($z = 3$ cm: open circles), as a function of the rf power P_{RF}.

Fig. 5. Here no results are plotted for the rf power of 600 - 1000 W because of the difficult identification of the accelerated group of ions. Within the rf power (100 - 500 W) for which the accelerated ions are detected at least, the energy of the ion beam is found to be constant although the density ratio of the beam ions to the bulk ions appears to decrease as presented in Fig. 4.

In the present experiments, the supersonic ion beam is detected at the downstream side of the source exit in the solenoid-free, magnetically expanding plasma using only the PMs, where the maximum of the plasma density inside the source is observed to be about 10^{12} cm^{-3} for the rf power of 1 kW. However, the accelerated ion beam could barely be detected for high-powered operation of the source. We now guess that the dissipation of the ion beam in the IEDF is caused by below two factors. One is the dissipation of the DL due to the extra ionization near the DL for high-power rf heating. Another is due to an increase in the bulk ions caused by an ionization in the diffusion chamber, where the accelerated ions in the IEDF are buried under the bulk ions. These are discussed in the next section.

4. Discussions

In this section, the physical mechanisms of the ion-beam dissipation for high rf power are discussed. In order to verify the existence of the DL for high rf power, the local plasma potentials inside the source tube and in the diffusion chamber are measured for various rf power. Figure 6 shows the local plasma potentials ϕ_p measured inside the source tube at $z = -6$ cm (closed squares) and at the downstream side of the source exit at $z = 3$ cm (open circles), respectively, as a function of the rf power P_{RF}. The potential difference between the sides upstream and downstream of the source exit is found not to be changed by the rf power; we can deduce the DL still exists near the source exit and the upstream ions are accelerated into the downstream side by the potential difference even for high rf power above 600 W.

In the DL plasma maintained by the single source upstream of the DL, the upstream density ratio to the downstream density would be decided by only the potential drop of the DL due to the flux conservation of the ions. That is to say, the ratio of the upstream to downstream density would not be changed by the experimental parameter if the potential drop of the DL is not changed. Figure 7 shows the axial profiles of (a) the plasma density n_p and (b) the normalized density for $P_{RF} = 200$ W (open squares) and 600 W (closed squares), respectively, where the potential drop of the DL for both cases are about 20 V as shown in Fig. 6. It is found that the ratio of the upstream to downstream densities is found to become small for high rf power of $P_{RF} = 600$ W, compared with the case of $P_{RF} = 200$ W. Thus, we can deduce the extra ionization occurs in the diffusion chamber. The ionization would generate the downstream bulk ions which does not contribute to an increase in the thrust for the propulsion devices.

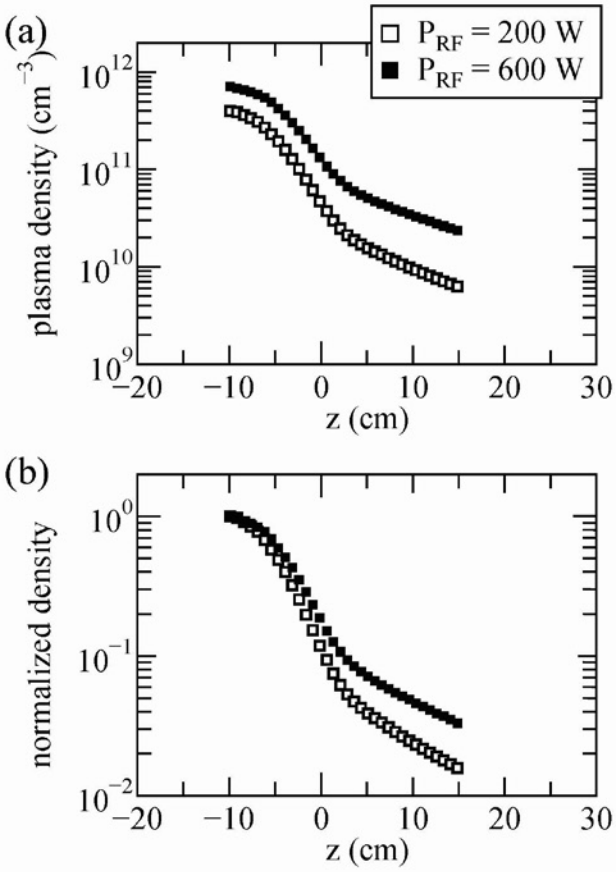

Fig. 7 Axial profiles of (a) the plasma density n_p and (b) the normalized density for $P_{RF} = 200$ W (open squares) and 600 W (closed squares).

Figure 8 shows the axial profiles of the amplitude of the magnetic fluctuation $|\tilde{B}|$ of 13.56 MHz, detected by the $\dot{B}$ probe for $P_{RF} = 200$ W (open squares) and 600 W (closed squares). Near fields created by the rf antenna for the plasma production is found to decrease exponentially along the z axis from the axial position ($z = -9$ cm) of the rf antenna. The upstream amplitude of the fluctuation for $P_{RF} = 600$ W is just a little higher than that for $P_{RF} = 200$ W, the factor of which is about 1.4; nevertheless the downstream fluctuation $|\tilde{B}|$ for $P_{RF} = 600$ W is about ten times of that for $P_{RF} = 200$ W. The downstream fluctuation would cause the extra ionization in the downstream of the DL and consequently create the bulk ions which bury the peak of the accelerated ions in the IEDFs. The details of the propagation of the fluctuation will be investigated from a viewpoint of the helicon wave

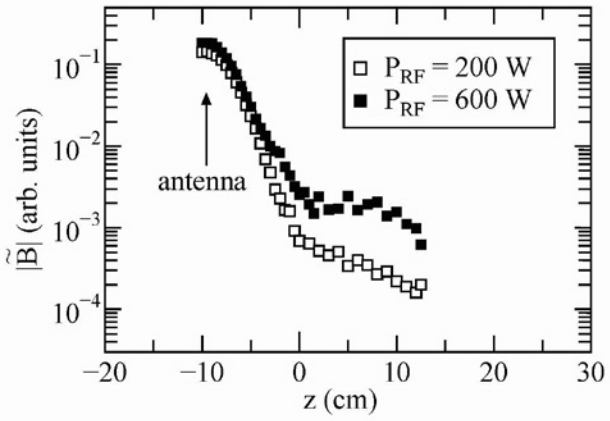

Fig. 8 Axial profiles of the magnetic fluctuation $|\tilde{B}|$ detected by the $\dot{B}$ probe for P_{RF} = 200 W (open squares) and 600 W (closed squares).

in the future.

5. Conclusion

The magnetically expanding plasma source using the PMs, which contains the electric DL near the source exit and generates the supersonic ion beam with the Mach number of about 2.6, is operated for high radiofrequency power of 13.56 MHz up to 1 kW. In the source tube, the divergent magnetic fields with the constant field of about 100 gauss inside the source tube and with the expanding field near the source exit are provided by the double concentric arrays of the PMs. The plasma density in the source tube can be increased up to 10^{12} cm^{-3} for 1 kW in the argon plasma, where the gas pressure is maintained at 1 mTorr. Under the conditions, the DL still exists although the signal of the accelerated ions are buried in the bulk ions in the IEDFs, which are extra created by the rf fields in the downstream side of the DL. In order to apply this source to the efficient propulsion device, the plasma-production area should be restricted only in the high-magnetic-fields side. The optimization of the source and the investigation of the wave propagating in the machine will be one of our next challenge for the application to the space propulsion.

Acknowledgements

This work is partially supported by a Grant-in-Aid for Young Scientists (B, 20740317) from the Ministry of Education, Culture, Sports, Science and Technology, Japan. This work is also partially supported by Yazaki Memorial Foundation for Science and Technology, and the Foundation for the Promotion of Ion Engineering.

[1] J. P. Squire, F. R. Chang Diaz, V. T. Jacobson, G. E. McCaskill, R. D. Bengtson, and R. H. Goulding, *Proceedings of 36th AIAA/ASME/SAE/ASEE Joint Propulsion Conference*, Alabam, 2000 (AIAA), p. 3752.
[2] K. Toki, S. Shinohara, T. Tanikawa, T. Hada, I. Funaki, K. P. Shamrai, Y. Tanaka, and A. Yamaguchi, J. Plasma Fusion Res. SERIES. **8**, 25 (2009).
[3] C. Charles, Plasma Sources Sci. Technol. **16** R1 (2007) and references therein.
[4] A. Meige, R. W. Boswell, C. Charles, and M. M. Turner, Phys. Plasmas **12**, 052317 (2005).
[5] K. Takahashi, C. Charles, R. W. Boswell, T. Kaneko, and R. Hatakeyama, Phys. Plasmas **14**, 114503 (2007).
[6] K. Takahashi, C. Charles, R. W. Boswell, and R. Hatakeyama, Phys. Plasmas **15**, 074505 (2008).
[7] K. Takahashi, C. Charles, R. W. Boswell, W. Cox, and R. Hatakeyama, Appl. Phys. Lett. **94**, 191503 (2009).
[8] H. Kuninaka, K. Nishiyama, I. Funaki, T. Yamada, Y. Shimizu, and J. Kawaguchi, J. Space Tech. Sci. **22**, 1 (2006).
[9] C. Charles, J. Phys. D : Appl. Phys. **42**, 163001 (2009) and references therein.
[10] F. F. Chen, Plasma Phys. Control. Fusion **33**, 339 (1991).
[11] R. W. Boswell and F. F. Chen, IEEE Trans. Plasma Sci. **25**, 1229 (1997).
[12] S. Shinohara, T. Hada, T. Motomura, K. Tanaka, T. Tanikawa, K. Toki, Y. Tanaka, and K. P. Shamrai, Phys. Plasmas **16**, 057104 (2009).
[13] I. S. Hong, Y. S. Hwang, G. H. Lee, D. Y. Kim, H. Y. Won, G. S. Eom, and W. Choe, Rev. Sci. Instrum. **71**, 1385 (2000).
[14] K. Sasaki, H. Kokubu, D. Hayashi, and K. Kadota, Thin Solid Films **386**, 243 (2001).
[15] K. P. Shamrai, Y. V. Virko, V. F. Virko, and A. I. Yakimenko, in *Proceedings of the 42nd AIAA/ASME/SAE/ASEE Joint Propulsion Conference and Exhibit*, California, 2006 (AIAA, New York, 2006), p. 4845.
[16] F. F. Chen and H. Torreblanca, Plasma Phys. Control. Fusion **49**, A81 (2007).
[17] F. F. Chen and H. Torreblanca, Phys. Plasmas **16**, 057102 (2009).
[18] K. Takahashi, K. Oguni, H. Yamada, and T. Fujiwara, Phys. Plasmas **15**, 084501 (2008).
[19] K. Takahashi and T. Fujiwara, Appl. Phys. Lett. **94**, 061502 (2009).
[20] K. Takahashi, T. Kaneko, and R. Hatakeyama, Plasma Sources Sci. Technol. **15**, 495 (2006).
[21] M. A. Lieberman and A. J. Lichtenberg, *Principles of Plasma Discharges and Materials Processing*, 2nd ed. (Wiley-Interscience, Hoboken, 2005), p.188.
[22] K. F. Schoenberg, Rev. Sci. Instrum. **49**, 1377 (1978).
[23] C. M. Franck, O. Grulke, and T. Klinger, Phys. Plasmas **10**, 323 (2003).
[24] Y. Sakawa, H. Kunimatsu, H. Kikuchi, Y. Fukui, and T. Shoji, Phys. Plasmas **11**, 286 (2004).
[25] C. Charles and R. W. Boswell, Phys. Plasmas **11**, 1706 (2004).